ACS APPLIED MATERIALS & INTERFACES

Research Article

www.acsami.org

Chlorin e6 Conjugated Poly(dopamine) Nanospheres as PDT/PTT Dual-Modal Therapeutic Agents for Enhanced Cancer Therapy

Da Zhang,[†,‡] Ming Wu,[†,‡] Yongyi Zeng,[†,‡,§] Lingjie Wu,[†,‡] Qingtang Wang,[†,‡] Xiao Han,[∥] Xiaolong Liu,*[,†,‡] and Jingfeng Liu*[,†,‡,§]

[†]The United Innovation of Mengchao Hepatobiliary Technology Key Laboratory of Fujian Province, Mengchao Hepatobiliary Hospital of Fujian Medical University, Fuzhou 350025, People's Republic of China

[‡]The Liver Center of Fujian Province, Fujian Medical University, Fuzhou 350025, People's Republic of China

[§]Liver Disease Center, The First Affiliated Hospital of Fujian Medical University, Fuzhou 350005, People's Republic of China

[∥]Biotechnology Research Institute, Chinese Academy of Agricultural Sciences, Beijing 100081, People's Republic of China

Supporting Information

ABSTRACT: Photodynamic therapy (PDT), using a combination of chemical photosensitizers (PS) and light, has been successfully applied as a noninvasive therapeutic procedure to treat tumors by inducing apoptosis or necrosis of cancer cells. However, most current clinically used PS have suffered from the instability in physiological conditions which lead to low photodynamic therapy efficacy. Herein, a highly biocompatible poly(dopamine) (PDA) nanoparticle conjugated with Chlorin e6 (referenced as the PDA-Ce6 nanosphere) was designed as a nanotherapeutic agent to achieve simultaneous photodynamic/photothermal therapy (PDT/PTT). Compared to the free Ce6, the PDA-Ce6 nanosphere exhibited significantly higher PDT efficacy against tumor cells, because of the enhanced cellular uptake and subsequently greater reactive oxygen species (ROS) production upon laser irradiation at 670 nm. Meanwhile, the PDA-Ce6 nanosphere could be also used as a photoabsorbing agent for PTT, because of the excellent photothermal conversion ability of PDA nanoparticle under laser irradiation at 808 nm. Moreover, our prepared nanosphere had extremely low dark toxicity, while excellent phototoxicity under the combination laser irradiation of 670 and 808 nm, both *in vitro* and *in vivo*, compared to any single laser irradiation alone. Therefore, our prepared PDA-Ce6 nanosphere could be applied as a very promising dual-modal phototherapeutic agent for enhanced cancer therapy in future clinical applications.

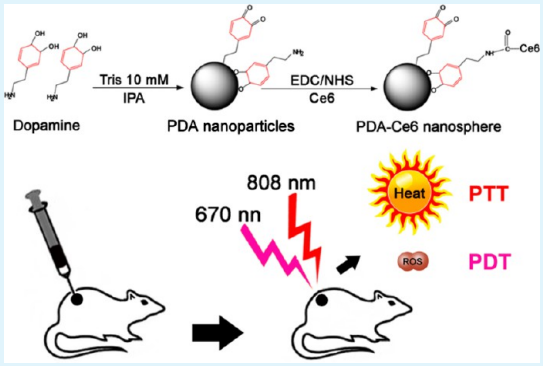

KEYWORDS: *poly(dopamine) nanoparticles (PDA NPs), Chlorin e6 (Ce6), photodynamic therapy (PDT), photothermal therapy (PTT), cancer therapy*

INTRODUCTION

Photodynamic therapy (PDT), as a noninvasive therapeutic modality, has obtained regulatory approval for clinical applications for various diseases such as age-related macular degeneration (AMD),[1] psoriasis,[2] and certain oncological diseases.[3,4] The concept of PDT is that the photosensitizer (PS) transfers the photon energy to generate reactive oxygen species (ROS) including Type I (superoxide anion, hydroxyl radical, and hydrogen peroxide) and Type II (singlet oxygen) upon the irradiation with appropriate wavelengths, and it is generally accepted that the Type II ROS is primarily responsible for cell death. Chlorins from "Chlorophyll a" have been frequently used as a PS agent, because of their high extinction coefficient in the red light region and high singlet oxygen quantum yield.[5] Among them, Chlorin e6 (Ce6) has been widely used for PDT, because of its activation by NIR light, relatively rapid elimination from the body, and high singlet oxygen generation efficiency.[6] Moreover, Ce6 could be further used as a NIR fluorescence imaging dye in the spectral range of 650−900 nm[7] to avoid the interference of endogenous chromophores within the body.[8] However, it is worth noting that Ce6 has low stability in physiological conditions, which significantly reduces the fluorescent quantum yield (Φ_f) and lowers the photosensitizing efficiency.[9] Therefore, the current emphasis on efforts to overcome the above-mentioned obstacles has resulted in the development of alternative or next-generation photosensitizers. With the aim of improving the efficiency of PDT, carbon-based, polymer-based, and lipid/liposome-based nanocarriers have been developed as an emerging platform for delivering Ce6,[10−13] while still suffering from the low drug loading amount and the inevitable release of the active dye before reaching its targets *in vivo*, which lead to the insufficient drug dose at the tumor site.[14] Therefore, it is of great interest to develop stable delivery vehicles as well as

Received: February 3, 2015
Accepted: April 3, 2015
Published: April 3, 2015

DOI: 10.1021/acsami.5b01027
ACS Appl. Mater. Interfaces 2015, 7, 8176−8187

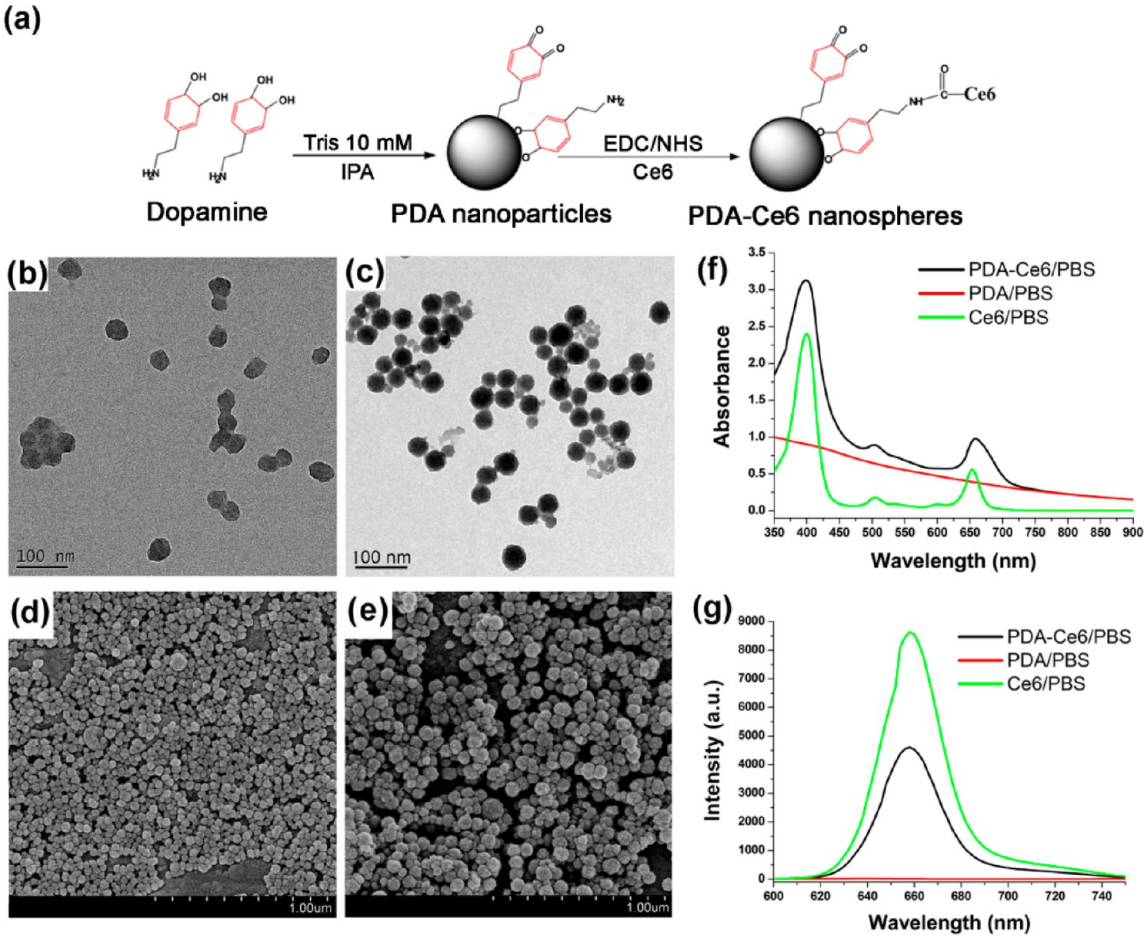

Figure 1. (a) Schematic view of the PDA-Ce6 nanospheres preparation procedure; (b) representative TEM image of PDA nanoparticles (scale bar = 100 nm); (c) representative TEM image of the prepared PDA-Ce6 nanospheres (scale bar = 100 nm); (d) representative SEM image of PDA nanoparticles (scale bar = 1 μm); and (e) representative SEM image of PDA-Ce6 nanospheres (scale bar = 1 μm). Also shown are (f) the vis−NIR spectra of the free Ce6, PDA nanoparticles, and PDA-Ce6 nanospheres in PBS; and (g) the fluorescence spectra of the free Ce6, PDA nanoparticles, and PDA-Ce6 nanospheres in PBS.

effectively integrate with other therapeutic modalities in a single agent to further improve the cancer therapy efficiency.

In recent years, photothermal therapy (PTT) has been explored as another noninvasive efficient treatment for malignant carcinomas. Following NIR laser irradiation, photoabsorbing agents could convert electromagnetic wave energy to local heat to produce hyperthermia and subsequently destroy tumors. Several types of photoabsorbing agents, such as indocyanine green (ICG),[15] carbon-based nanomaterials,[16,17] golden-based nanomaterials,[18,19] Prussian Blue nanoparticles (NPs),[20] and Pd (palladium) nanosheets[21] have been developed for cancer photothermal treatment. Furthermore, recent advances in nanotechnology allow us to combine the PTT treatment and PDT treatment in a single platform to further enhance the therapeutic efficiency for malignant carcinomas, because of the synergistic effects. For example, Boris Khlebtsov's group developed a dual-modal tumor therapeutic agent by combining the photodynamic treatment and photothermal treatment through loading hematoporphyrin into the silica shell of gold nanorods, and the combined treatment resulted in significantly enhanced cancer therapy, when compared to any of the single treatments.[22] Chen's group also reported that the Chlorin e6 (Ce6)-functionalized gold nanostars (GNS-PEG-Ce6) combine the PDT treatment with PTT treatment to enhance the cancer therapy efficiency.[23]

In addition to above-mentioned photothermal ablation agents, poly(dopamine) (PDA), as a well-known polymer coatings material, has also been used recently as a photothermal agent for cancer therapy.[15,24−27] PDA nanoparticles that can be obtained from the self-polymerization of dopamine under alkaline conditions (pH >7.5), with oxygen as the oxidant, exhibit excellent photothermal conversion efficiency (40%) with the advantages of good biocompatibility, no cytotoxicity, and excellent dispersibility in aqueous solution.[26] Meanwhile, the existence of functional groups (i.e., catechol and amine) on the surface of PDA makes it suitable for further conjugation or modification. Herein, we reported the construction of PDT/PTT dual-modal therapeutic agents through the covalent conjugation of Ce6 onto the surface of PDA nanoparticles (referred as PDA-Ce6 nanoparticles) for enhancing the cancer therapy efficiency (Figure 1a), in which the PDT function was originated from the conjugated Ce6 and the PTT function was originated from PDA nanoparticles, respectively.

EXPERIMENTAL SECTION

Materials. Dopamine hydrochloride (DA·HCl), Chlorin e6 (Ce6), *N*-(3-dimethylamino-propyl)-*N*-ethylcarbodiimide hydrochloride (EDC), *N*-hydroxysuccinimide (NHS), 9,10-anthracenediylbis (methylene) dimalonic acid (ABDA), and 2′,7′-dichlorodihydrofluorescein diacetate (DCFH-DA) were purchased from Sigma−Aldrich. Calcein-

DOI: 10.1021/acsami.5b01027
ACS Appl. Mater. Interfaces 2015, 7, 8176−8187

AM was purchased from J&K Scientific. An Annexin V-fluoroisothiocyanate (FITC) apoptosis detection kit and a Cell Counting Kit-8 (CCK8) were purchased from Dojindo Laboratories (Kumamoto, Japan). Deionized water with a resistivity of 18.2 MΩ cm was obtained from a Milli-Q Gradient System (Millipore, Bedford, MA, USA) and used for all experiments. Unless specified, all other chemicals were commercially available and used as received.

Cell Culture. The human hepatocellular carcinoma cancer cell line HepG2, and the normal human hepatocyte cell line Chang liver were maintained as monolayer cultures in RPMI-1640 medium supplemented with 10% fetal bovine serum (FBS, Atlanta Biologicals, Lawrenceville, GA, USA) and 1% penicillin-streptomycin (Gibco BRL, Grand Island, NY, USA) at 37 °C in a humidity atmosphere (5% CO_2).

Synthesis of the PDA-Ce6 Nanospheres. Poly(dopamine) nanoparticles were prepared as follows. Briefly, tris-HCl (60.26 mg, 10 mM) was dissolved in the mixture of 50 mL of deionized water and 10 mL of isopropanol (IPA), and then the pH of the mixture solution was adjusted to 8.5. Then, 25 mg of dopamine powder was added into the mixture under vigorous stirring. After continuously stirring for 4 days, the poly(dopamine) nanoparticles were collected by centrifugation at 40 000 g for 20 min, and then washed twice with deionized water and ethyl alcohol, respectively. The obtained PDA nanoparticles were dispersed in water for further usage.[28] The PDA-Ce6 nanospheres were prepared as follows. Briefly, 1 mg of Ce6 was dissolved in 1 mL of dimethylsulfoxide (DMSO); then, 12 mg of EDC and 24 mg of NHS were further added into the Ce6 solution and kept reacting for 4 h with stirring at room temperature. Afterward, the reacted mixture was added dropwise into 1 mL of PDA aqueous solution (1 mg/mL); after further shaking for 24 h at 4 °C, the crude product was collected by centrifugation at 30 000 g for 20 min and sequentially washed with ethyl alcohol and deionized water to remove the excess of Ce6, EDC, and NHS. The finally obtained PDA-Ce6 nanospheres were resuspended in deionized water or PBS solution for further usage. The conjugation amount of Ce6 on the surface of PDA nanospheres (CM) was calculated using the following equation:

$$\mathrm{CM}\,(\%) = \frac{M_\mathrm{F} - M_\mathrm{S}}{M_\mathrm{PDA} + M_\mathrm{F} - M_\mathrm{S}} \times 100$$

where M_F is the feeding amount of free Ce6, M_S is the amount of free Ce6 in the collected supernatant, and M_PDA is the feeding amount of PDA. To measure M_S, 1 mL of collected supernatant was analyzed by HPLC (Model Agilent 1260 Infinity, Agilent Technologies, Germany) using Agilentzorbax Eclipse Plus C18 column (4.6 mm × 100 mm, 3.5 μm, Agilent Technologies, USA) with following experimental conditions: the column temperature was maintained at 30 °C; the mobile phase is consisted of ethanol in 0.05 mol L^{-1} ammonium acetate aqueous solution (62/38, volume ratio) at a flow rate of 0.7 mL/min and pH of 5.5. The Ce6 concentration was determined by the absorption intensity at 400 nm.[29] The correlation between the peak area at the retention time of 11.66 min (see Figure S5a in the Supporting Information) and the concentration of Ce6 was analyzed by linear regression, which showed a well-correlated linear relationship (R^2 = 0.9923). As shown in Figure S5b in the Supporting Information, the standard curve has a very good linear relation with Ce6 from the concentration of 1−8 μg/mL (Y = 10.721X + 0.0134). Based on our HPLC analysis, M_S was determined to be 0.743 mg, where M_F and M_PDA was 1 mg and 1 mg, respectively; therefore, the CM value was calculated to be 20.44%.

Characterization of the PDA-Ce6 Nanospheres. Elemental analysis of PDA nanoparticles was carried out through a Vario ELIII elemental analyzer. Solid-state ^{13}C CP-MAS NMR spectra of PDA nanoparticles was collected at 100.5 MHz, on a Bruker Avance II 400 spectrometer operating at a static field of 9.4 T, equipped with a 4 mm MAS probe. Samples were finely ground in a mortar and packed into 4-mm zirconia rotors sealed with Kel-F caps. The spinning speeds were set at 8 kHz. FT-IR spectrum of the prepared PDA nanoparticles was collected on a FT-IR spectrometer (Perkin−Elmer, USA). The samples were mixed with KBr, compressed to a plate, and evaluated over the spectral region of 400−4000 cm^{-1}. The vis-NIR absorbance of the PDA-Ce6 nanospheres was measured by a vis-NIR spectrometer (Beijing Perkinje General Instrument Co., China). TEM was performed by using a Model JEM-2010 electron microscope (JEOL, Japan) to characterize the overall morphology and the chemical compositions of the sample. The dynamic light scattering (DLS) experiments were performed at 25 °C on a Zetasizer NanoZS system (Malvern Instruments, Malvern U.K.) with a detection angle of 173° and a 3 mW He−Ne laser operating at the wavelength of 633 nm. Briefly, 1 mL of PDA or PDA-Ce6 nanospheres dispersion (0.1 mg/mL in deionized (DI) water) was placed into a glass cuvette, then the sample was measured. The average value was obtained from three replicated measurements for each sample. The PDI values were obtained by analyzing the correlation functions through cumulative analysis. Zeta potential measurements were performed at 25 °C on the Zetasizer NanoZS device, using the M3-PALS technology.

Measurements of ROS Generation under Laser Irradiation at 670 nm. ROS generation of the PDA-Ce6 nanospheres was measured by using ABDA as an indicator. Briefly, the PDA-Ce6 in PBS (Ce6: 6 μg/mL) containing 20 mM ABDA was irradiated by a 670 nm laser with a power intensity of 50 mW/cm^2, a 808 nm laser with a power intensity of 2 W/cm^2, or combined laser irradiation under 670 nm (50 mW/cm^2) and 808 nm (2 W/cm^2) simultaneously for 0, 4, 8, 12, 16, and 20 min, respectively; afterward, the absorbance change of ABDA was measured using a UV−vis spectrometer (Beijing Perkinje General Instrument Co., China).

Temperature Elevation Induced by Laser Irradiation at 808 nm. To study the photothermal effect of the PDA-Ce6 nanospheres, 2 mL of aqueous solution with various concentrations of the nanospheres was irradiated by an 808 nm laser with a power density of 2 W/cm^2. The temperature of the solution was monitored by a thermocouple microprobe (Φ = 0.5 mm) (STPC-510P, Xiamen Baidewo Technology Co., China) that was submerged in the solution every 10 s.

Confocal Microscopy Studies of the PDA-Ce6 Nanospheres Uptake. The uptake of PDA-Ce6 nanospheres by HepG2 cells was investigated using confocal microscopy. HepG2 cells (5×10^4) were seeded onto 35 mm glass-bottom Petri dishes and cultured for 24 h at 37 °C in the incubator. The PDA-Ce6 nanospheres then were added to the cells and further incubated for 2 h. Subsequently, the HepG2 cells were washed three times with PBS (pH 7.4) and then fixed with 4% paraformaldehyde for 15 min. Finally, the cells were imaged by a confocal microscope (Nikon A1R-AI confocal microscope system) with laser excitation at 543 nm for Ce6.

***In Vitro* Cellular Uptake Measured by Flow Cytometry.** HepG2 cells were seeded in six well plates at a density of 1×10^6 cells per well and incubated in a humid 5% CO_2 atmosphere for 24 h. The original medium then was replaced with fresh culture medium containing free Ce6 or PDA-Ce6 nanospheres (Ce6 concentration: 2.5 or 5 μg/mL). After incubating for 2 h, the cells were washed three times with cold PBS, and then dispersed in 1 mL of PBS. Finally, the cells were filtered through a 40 μm nylon mesh to remove cell aggregates before fluorescence-activated cell sorting (FACS) analysis. Fluorescence measurement of the intracellular Ce6 was done in the FL4 channel with the excitation at 670 nm.

***In Vitro* Cytotoxicity and Photodynamic/Photothermal-Induced Cell Death.** The cytotoxicity of PDA-Ce6 nanospheres was evaluated on HepG2 cells and Chang liver cells using a Cell Counting Kit (CCK8). The cells were seeded in a 96-well plate at a density of 1×10^5 cells per well and incubated in a humid atmosphere (with 5% CO_2) for 24 h. The original medium then was replaced with fresh culture medium containing PDA-Ce6 nanospheres at a final Ce6 concentration of 0.1−8 μg/mL. Meanwhile, the cells incubated with cell culture medium only were prepared as untreated control. The medium was aspirated after 24 h of incubation, and the cells were washed twice with 100 μL PBS solution to remove noninternalized nanoparticles. Subsequently, 100 μL of culture medium and 10 μL of CCK8 solution (5 mg/mL in PBS solution) were added to the wells. After incubation for 2 h at 37 °C, the absorbance of the solution in each well at 450 nm was measured with a microplate reader (Spectra

DOI: 10.1021/acsami.5b01027
ACS Appl. Mater. Interfaces 2015, 7, 8176−8187

Max M5). The proliferation of cells was determined by the absorption intensity. Cell viability was expressed as follows:

$$\text{cell viability}\,(\%) = \frac{\text{OD}_{\text{sample}} - \text{OD}_{\text{blank}}}{\text{OD}_{\text{control}} - \text{OD}_{\text{blank}}} \times 100$$

Here, $\text{OD}_{\text{sample}}$ and $\text{OD}_{\text{control}}$ are the absorbance values of the treated cells (as indicated) and the untreated control cells (without nanoparticles), respectively. The OD_{blank} was the absorbance of CCK8 reagent itself at 450 nm. All experiments were performed in quadruplicate.

CCK-8 was also used to study the photodynamic/photothermal cell toxicity of PDA-Ce6 nanospheres against HepG2 cells. In a typical experiment, HepG2 cells were first seeded into a 96-well plate at a density of 1×10^4 cells per well at 37 °C in a 5% CO_2 atmosphere for 24 h. The cells then were washed three times with PBS to remove dead cells, followed by incubation with different concentrations of PDA-Ce6 dispersed in RPMI-1640 medium at 37 °C for 2 h. Next, the cells were washed three times with PBS to remove free NPs. Then, fresh culture medium was added, and the cells were exposed to 808 nm laser (2 W/cm^2) for 5 min (PTT irradiation), or 670 nm laser (50 mW/cm^2) for 5 min (PDT irradiation), or the combination of the PDT/PTT irradiation (5 min of each), respectively. After laser irradiation, the cells were incubated with fresh RPMI-1640 culture medium containing 10% fetal bovine serum at 37 °C for 24 h. The cell viability then was determined by CCK8, according to the above-mentioned procedure.

To further evaluate cell apoptosis induced by the photothermal/photodynamic treatment of PDA-Ce6 nanospheres, we used the Annexin-V-FITC/propidium iodide (PI) staining method. HepG2 cells were first seeded into a 48-well plate at a density of 1×10^4 cells per well at 37 °C in a 5% CO_2 atmosphere for 24 h. The cells then were washed three times with PBS to remove dead cells, followed by incubation with PDA-Ce6 nanospheres (Ce6, 1 μg/mL) that were dispersed in a culture medium at 37 °C for 2 h. Next, the cells were washed by culture medium to remove the none uptaken nanospheres, and then exposed to 808 nm laser (2 W/cm^2) for 5 min (PTT irradiation), or 670 nm laser (50 mW/cm^2) for 5 min (PDT irradiation), or the combination of the PDT/PTT irradiation (5 min of each), respectively. After laser irradiation, the cells were incubated with fresh culture medium at 37 °C for 24 h. The cells then were collected and resuspended in 500 μL of binding buffer, and Annexin V-FITC and PI were added, following the manufacturer's recommendation. Samples were incubated in darkness for 15 min at room temperature and then analyzed using flow cytometry.

Tumor Xenograft and *In Vivo* Photodynamic/Photothermal Cancer Therapy. Male BALB/c-nude mice (6 weeks old) were purchased from China Wushi, Inc. (Shanghai, China). All animal procedures were approved by the Animal Ethics Committee of Fujian Medical University. Tumor-bearing mice were prepared by subcutaneously injecting a suspension of the HepG2 cells (10^7 cells) in sterilized 1× PBS. When the tumor size reached ~120 mm^3, PDA-Ce6 nanospheres (20 μg/mL PDA and 5 μg/mL Ce6; 200 μL injection of each mouse) were directly injected into the tumor site. One group of mice treated with the same volume of sterilized PBS was taken as the control group. The mice were segregated into four groups:

(1) sterilized PBS with combined laser irradiation simultaneously under 670 nm (50 mW/cm^2) and 808 nm (2 W/cm^2) for 10 min (n = 5);
(2) PDA-Ce6 nanospheres with single laser irradiation under 670 nm (50 mW/cm^2) for 10 min;
(3) PDA-Ce6 nanospheres with single laser irradiation under 808 nm (2 W/cm^2) for 10 min; and
(4) PDA-Ce6 nanospheres with combined laser irradiation under 670 nm (50 mW/cm^2) and 808 nm (2 W/cm^2) simultaneously for 10 min.

The irradiation was conducted after 24 h of injection. The therapeutic effects were evaluated by monitoring the tumor volume and body weight changes in each group every 2 days, up to 14 days. The tumor size was measured using caliper every other day after the treatment. The tumor volume (V) was calculated using the following equation:

$$V = \frac{AB^2}{2}$$

where A and B are the longer and shorter diameter (mm) of the tumor, respectively. Meanwhile, to examine the histological changes of the tumors, one tumor-bearing mouse in each group was sacrificed after 24 h of irradiation, and the tumors were collected, then stained with Hematoxylin and eosin (H&E) for histopathology evaluation and Ki67 antibody for immunohistochemical analysis.

RESULTS AND DISCUSSION

Synthesis and Characterization of PDA-Ce6 Nanospheres. The synthesis procedures of PDA-Ce6 nanospheres have been illustrated in Figure 1a. First, poly(dopamine) nanoparticles (PDA NPs) were synthesized by self-polymerization of dopamine (DA) under alkaline conditions (pH 8.5) with oxygen as the oxidant in the DI water/IPA mixture with a volume ratio of 5:1. Transmission electron microscopy (TEM) (Figure 1b) and scanning electron microscopy (SEM) (Figure 1d) revealed the average diameter of PDA nanoparticles was 42 ± 2 nm. Elemental analysis of PDA nanoparticles has shown a composition of 50.47% C, 5.35% H, and 8.70% N. ^{13}C cross-polarization/magic-angle-spinning (CP/MAS) spectra of PDA nanoparticles (Figure S1 in the Supporting Information) exhibited less-intense aliphatic resonances at $\delta \approx 30$ and 40 ppm, and relatively well-resolved bands in the sp^2 region at $\delta \approx$ 115, 130, and 145 ppm, revealing a substantial proportion of cyclized units. The presence of resonances at $\delta \approx 170$ ppm suggested some carboxylic acid groups and/or other carbonyl-type groups generated at the expense of OH-bearing carbons via oxidative fission of catechol moieties. The presence of an intense signal at $\delta \approx 60$ ppm in the spectrum indicated incorporation of the buffer (Tris). These results are consistent with the PDA structure comprising uncyclized (catecholamine) and cyclized (indole) units, pyrrole carboxylic acid moieties, and the covalent incorporation of Tris buffer, which has been reported by Vecchia et al.[30] Fourier transform infrared (FT-IR) spectroscopy was also conducted to explore the structure of PDA nanoparticles. As shown in Figure S2 in the Supporting Information, PDA nanoparticles presented a specific absorption features, including the bands at 1494 and 3200 cm^{-1} attributed to aromatic rings and catechol −OH groups, respectively, and this spectrum is in accordance with the reported literature.[26,31]

Next, Ce6 was covalently bound to the amino groups on the surface of PDA nanoparticles by a conventional carbodiimide reaction through the use of EDC and NHS. As shown in Figures 1c and 1e, after conjugation of Ce6, the average diameter of the PDA nanospheres was increased to 49 ± 3 nm. Dynamic light scattering (DLS) showed a relatively narrow size distribution, and the average sizes of PDA and PDA-Ce6 were 91.1 ± 3.19 nm and 138.1 ± 4.31 nm, respectively (see Figure S3 in the Supporting Information). The larger of the hydrodynamic size than those determined by TEM and SEM were most likely due to the nanoparticles under different dry and wet conditions, as well as the small aggregation in solution. To investigate the change of the surface charge of the PDA nanoparticles after Ce6 conjugation, the zeta potential of the PDA and PDA-Ce6 was determined. As shown in Figure S4 in the Supporting Information. Zeta potential results showed that the PDA nanoparticles in water had a negative surface charge (−23.4 ± 1.9 mV), which could be ascribed to the

DOI: 10.1021/acsami.5b01027
ACS Appl. Mater. Interfaces 2015, 7, 8176−8187

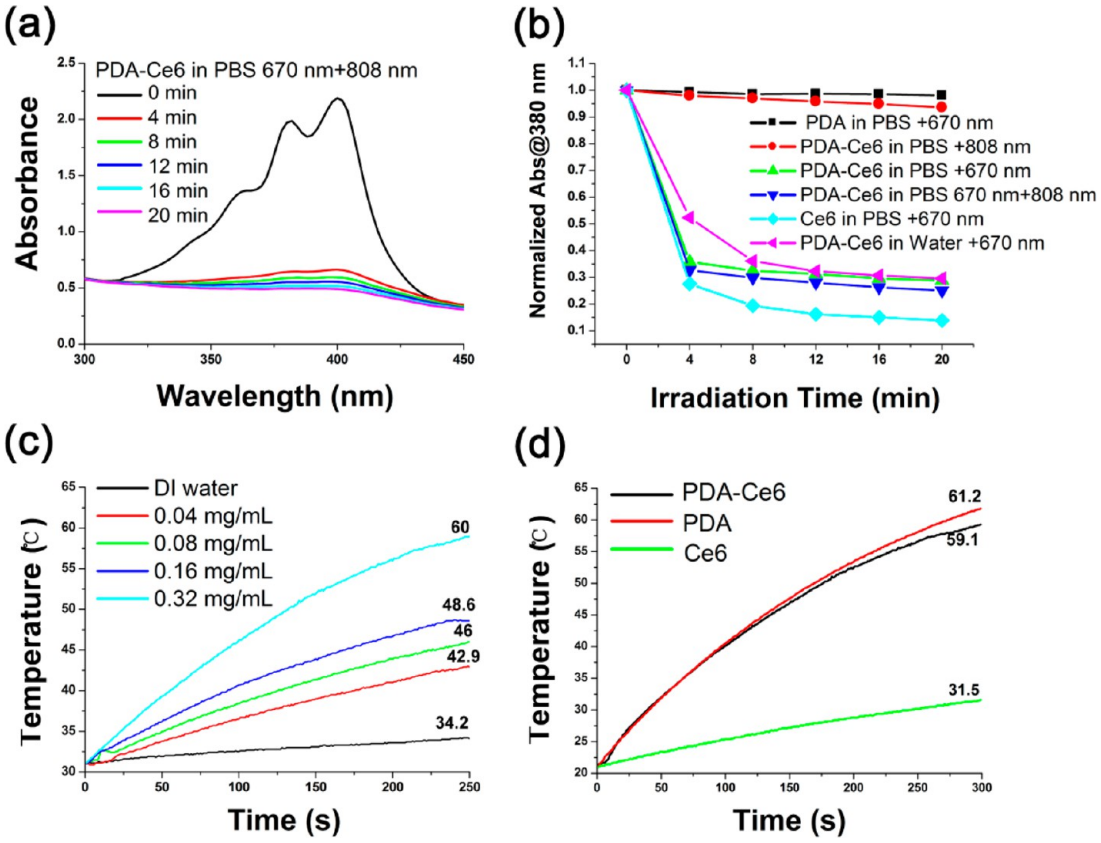

Figure 2. (a) Absorbance of 9,10-dimethylanthracene (ABDA, 20 mM) after photodecomposition by ROS generation upon NIR laser irradiation (670 nm (50 mW/cm^2) + 808 nm (2 W/cm^2)) in the presence of the PDA-Ce6 nanospheres in PBS; (b) normalized absorbance of 9,10-dimethylanthracene (ABDA, 20 mM) at 380 nm during photodecomposition by ROS generation in the presence of PDA nanoparticles in PBS (670 nm (50 mW/cm^2)), PDA-Ce6 in PBS (808 nm (2 W/cm^2)), PDA-Ce6 in PBS (670 nm (50 mW/cm^2)), PDA-Ce6 in PBS (670 nm (50 mW/cm^2) + 808 nm (2 W/cm^2)), free Ce6 in PBS (670 nm (50 mW/cm^2)) and PDA-Ce6 in water (670 nm (50 mW/cm^2)), respectively. (c) Temperature elevation curves of deionized (DI) water and the PDA-Ce6 nanospheres with different concentrations. (d) Temperature elevation curves of free Ce6, PDA nanoparticles, and PDA-Ce6 nanospheres aqueous solutions at the same concentration of PDA or Ce6.

deprotonation of catechol −OH groups on the PDA.[31] However, after Ce6 conjugation, the surface charge of these nanoparticles became more negative (−28.03 ± 0.9 mV), because of the additive −COOH groups of the Ce6 binding onto the PDA. The successful conjugation of Ce6 onto PDA nanoparticles was confirmed by vis-NIR absorbance (Figure 1f) and fluorescence emission spectra (Figure 1g). Comparing to the absorbance of PDA nanoparticles, the PDA-Ce6 nanospheres in PBS exhibited new absorption peaks at 405 nm (Soret peak) and 675 nm (Q-band), corresponding to the characteristic absorption peak of Ce6, which indicated the successful conjugation of Ce6. Furthermore, the absorbance intensity of the PDA-Ce6 nanospheres was much higher than that of free Ce6 in PBS, which is ascribed to the additive effect of the absorbance of PDA from 350 nm to 900 nm. However, the fluorescence intensity of the PDA-Ce6 nanospheres was lower than the same amount of free Ce6 in PBS on the emission spectra at 675 nm, ascribing to the quenching effect of PDA nanoparticles.[25]

ROS Production and Temperature Elevation Induced by NIR Laser Irradiation. ROS generation, which is primarily responsible for the cell death, is the key parameter to estimate the PDT effect. Thus, we used 9,10-anthracenediyl-bis-(methylene) dimalonic acid (ABDA) as an indicator to evaluate the ROS production of PDA-Ce6 nanospheres induced by 670 nm, 808 nm, or combined (670 nm + 808 nm) laser irradiation.[32] As shown in Figures 2a and 2b, the PDA-Ce6 nanospheres exhibited a sharp decline in ABDA absorbance at the range from 300 nm to 400 nm under combined (670 nm + 808 nm) or 670 nm laser irradiation for 4 min, while there is no decrease of ABDA absorbance under 808 nm laser irradiation alone (Figure S6e in the Supporting Information), indicating that the single 670 nm laser irradiation could trigger the rapid ROS generation of PDA-Ce6 nanospheres while the 808 nm laser irradiation alone could not produce any ROS. To further confirm that the ROS is generated from the Ce6 of nanospheres, we compared the ROS production of PDA-Ce6 nanospheres with that of PDA nanospheres or free Ce6 at the equivalent concentration in PBS buffer under laser irradiation at 670 nm. As shown in Figures S6a−c in the Supporting Information and Figure 2b, PDA-Ce6 nanospheres and free Ce6 could produce significant amount of ROS, but the PDA nanospheres alone could not generate any ROS under the same conditions. Furthermore, we compared the ROS production of PDA-Ce6 nanospheres in water with that of free Ce6 in PBS. The results showed that the PDA-Ce6 nanospheres have a slightly slower and less ROS production (by ∼10%) than that of free Ce6, which might be due to the slight quenching of Ce6 by PDA (see Figures S6a and S6d in the Supporting Information, and Figure 2b). However, when the PDA-Ce6 nanospheres and free Ce6 were dissolved in PBS with 10% fetal bovine serum (FBS), the PDA-Ce6 nanospheres exhibited

DOI: 10.1021/acsami.5b01027
ACS Appl. Mater. Interfaces 2015, 7, 8176−8187

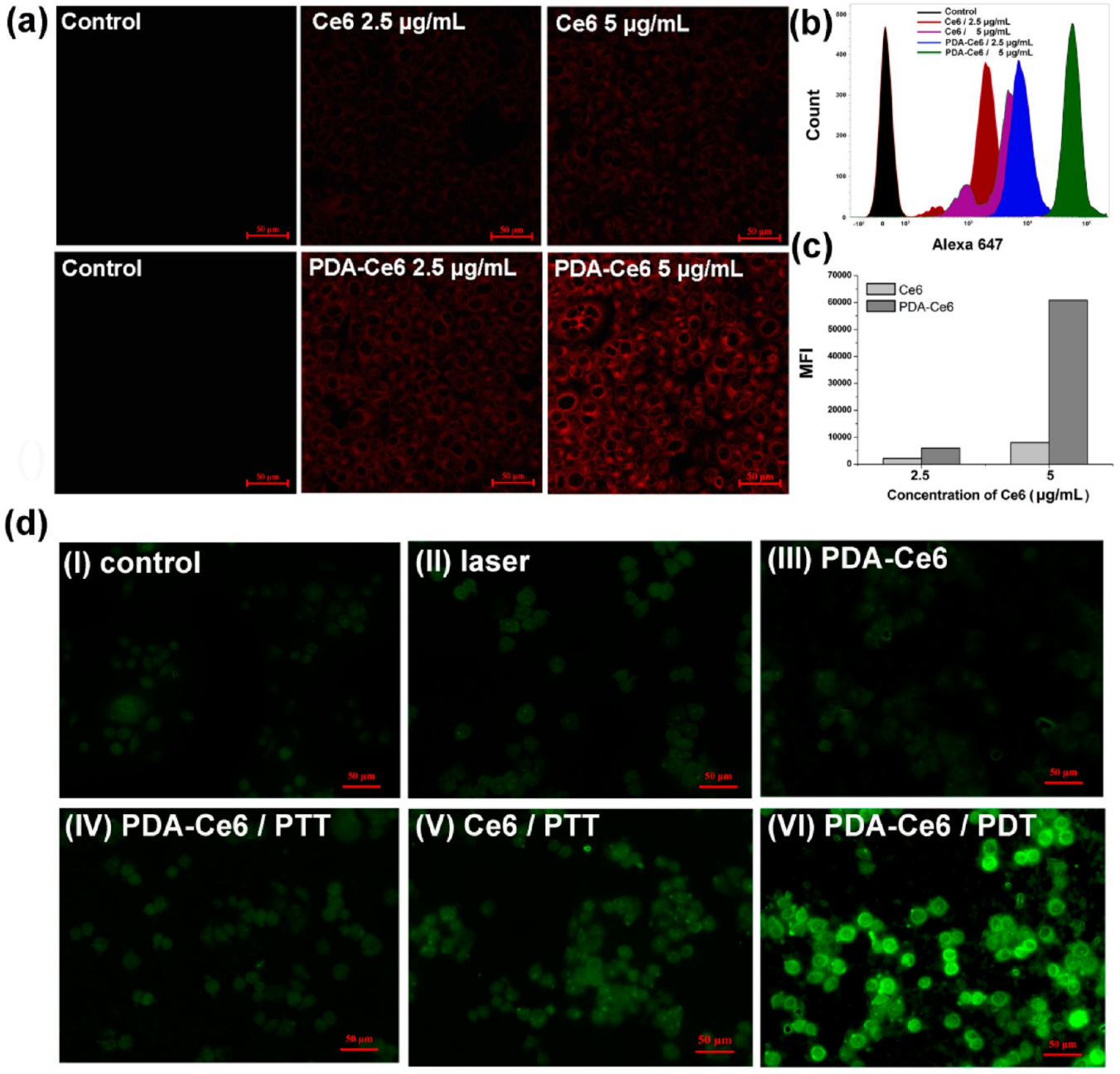

Figure 3. (a) Confocal images of HepG2 cells incubated with free Ce6 and PDA-Ce6 nanospheres for 2 h. Scale bar = 50 μm. (b) Flow cytometry analysis of Ce6 fluorescence inside the cells after incubation with free Ce6 or PDA-Ce6 for 2 h. (c) The mean fluorescence intensity (MFI) of Ce6 in each group as indicated, untreated HepG2 cells was taken as control. (d) Fluorescence microscopy images of HepG2 cells that received different treatments as indicated. Green color represents $^1O_2$ indicator DCFH-DA (scale bar = 50 μm). [Legend: (I) none treated cells as a control; (II) cells treated only with 670 nm laser irradiation; (III) cells treated with PDA-Ce6 without laser irradiation; (IV) cells treated with PDA-Ce6 with 808 nm laser irradiation; (V) cells treated with free Ce6 with 670 nm laser irradiation; and (VI) cells treated with PDA-Ce6 nanospheres with 670 nm laser irradiation.] The 808 nm laser power intensity is 2 W/cm^2, and the 670 nm laser power intensity is 50 mW/cm^2.

faster and stronger ROS generation (~20%) than that of free Ce6 (Figure S7 in the Supporting Information); this might be due to the fact that the free Ce6 can easily bind to FBS and lose its photodynamic activity, but the PDA-Ce6 nanospheres could be maintained in their free form.[33] These results suggested the higher photodynamic activity of our PDA-Ce6 nanospheres, compared to free Ce6.

In addition, the strong absorption of PDA-Ce6 nanospheres in the wavelength range of 650−900 nm might be further used for PTT treatment. In Figure 2c, following the laser irradiation at 808 nm, with a power intensity of 2 W/cm^2 for 250 s, the temperature of the PDA-Ce6 nanospheres, which contain 0.04, 0.08, 0.16, and 0.32 mg/mL of PDA increased up to 42.9, 46, 48.6, and 60 °C, respectively. For 0.32 mg/mL concentration, the temperature already increased up to 60 °C, which is sufficient to kill cancer cells. In contrast, the temperature of DI water showed slight changes when exposed to laser as a control. Meanwhile, as shown in Figure 2d, the temperature elevation of the equivalent amount of PDA-Ce6 nanospheres (59.1 °C) and PDA nanoparticles (61.2 °C) were much higher than that induced by free Ce6 (31.5 °C), indicating that the PDA nanoparticles were primarily responsible for the photothermal

DOI: 10.1021/acsami.5b01027
ACS Appl. Mater. Interfaces 2015, 7, 8176−8187

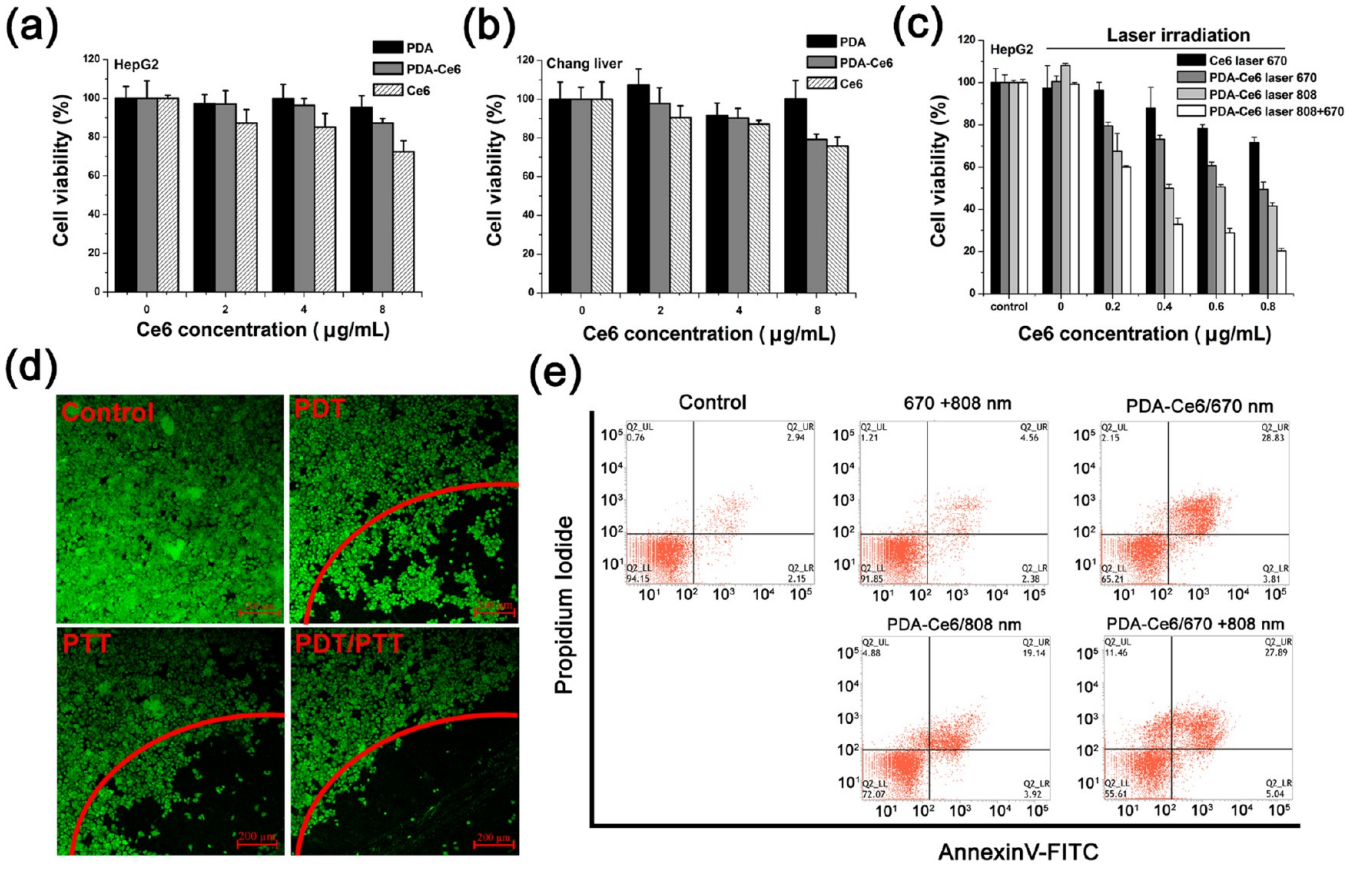

Figure 4. (a) Cell viability of HepG2 cells treated with different concentration of PDA-Ce6, PDA, and Ce6 without laser irradiation. (b) Cell viability of Chang liver normal liver cells treated with different concentration of PDA-Ce6, PDA, and Ce6 without laser irradiation. Bars denote the standard deviation (±SD, $n = 6$). (c) Cell viability of HepG2 cells treated with different concentration of PDA-Ce6 and Ce6 under PDT treatment (670 nm, 50 mW/cm^2), PTT (808 nm, 2 W/cm^2) treatment or combined PDT/PTT treatment, respectively. Bars denote the standard deviation (±SD, $n = 6$). (d) Fluorescence images of Calcein AM stained HepG2 cells incubated with PDA-Ce6 nanospheres (Ce6: 1 μg/mL) for 2 h, with PDT treatment (670 nm, 50 mW/cm^2), PTT (808 nm, 2 W/cm^2) treatment,or combined PDT/PTT treatment, respectively (scale bars = 50 μm). (e) Apoptosis of HepG2 cells incubated with 1 μg/mL PDA-Ce6 nanospheres under PDT treatment (670 nm, 50 mW/cm^2), PTT (808 nm, 2 W/cm^2) treatment or combined PDT/PTT treatment. The cells apoptosis were determined by flow cytometry analysis using Annexin V-FITC and PI staining.

conversion. These results clearly proved that our prepared PDA-Ce6 nanospheres have an excellent singlet oxygen generation and photothermal conversion ability.

Evaluation of the Cellular Uptake of PDA-Ce6 Nanospheres. In order to ensure the phototherapeutic efficacy of PDA-Ce6 nanospheres for cancer therapy, efficient internalization by cancer cells is of great importance. Here, confocal microscopy imaging was carried out to detect the internalization of PDA-Ce6 nanospheres. As shown in Figure 3a, the red fluorescence signal from the internalized PDA-Ce6 in HepG2 cells could be clearly seen after incubation with the PDA-Ce6 nanospheres (Ce6, 2.5 μg/mL), which demonstrates that our PDA-Ce6 nanospheres could be effectively internalized into HepG2 cells; however, the red fluorescence signal of the HepG2 cells incubated with the same concentration of free Ce6 was not so obvious. The similar results could also be observed when the concentration of Ce6 even increased to 5 μg/mL. These results were implied that the PDA-Ce6 nanospheres could be internalized more rapidly and effectively into the cancer cells through the endocytosis approach, than that of the free Ce6, which might be internalized into cells through passive diffusion. Furthermore, flow cytometry experiments were performed to quantify the internalization efficiency of the PDA-Ce6 nanospheres in HepG2 cells. As shown in Figure 3b, the mean fluorescence intensity (MFI) of the cells treated with PDA-Ce6 nanospheres (5940) was ∼2.77-fold higher than those incubated with free Ce6 (2146) at the same concentration (2.5 μg/mL of Ce6 for both). More obviously, when the Ce6 concentration increased up to 5 μg/mL, the PDA-Ce6 incubated HepG2 exhibited ∼10.5 times higher MFI than that of the free Ce6 incubated HepG2 cells at this equivalent concentration (Figure 3c). These results were very consistent with the confocal microscopy results, and they demonstrated that the PDA nanoparticles could be taken as a highly efficient nanocarrier for Ce6 delivery to the cancer cells.

Evaluation ROS Production of the Intracellular PDA-Ce6 Nanospheres upon NIR Laser Irradiation. Our previous results demonstrated that our PDA-Ce6 nanospheres could produce significant ROS under NIR laser irradiation in aqueous media. The increased amount of ROS generated by the PDA-Ce6 nanospheres could improve the oxidative damage to the cancer cells *in vitro*. Thus, the intracellular ROS production of PDA-Ce6 nanospheres in HepG2 cells was examined by using the 2′,7′-dichlorodihydrofluorescein diacetate (DCFH-DA) as a ROS fluorescence indicator. As shown in Figure 3d, the untreated control cells showed a slight green DCFH-DA fluorescence, indicating that only a few ROS were present inside the cancer cells. Meanwhile, either the laser irradiation

DOI: 10.1021/acsami.5b01027
ACS Appl. Mater. Interfaces 2015, 7, 8176−8187

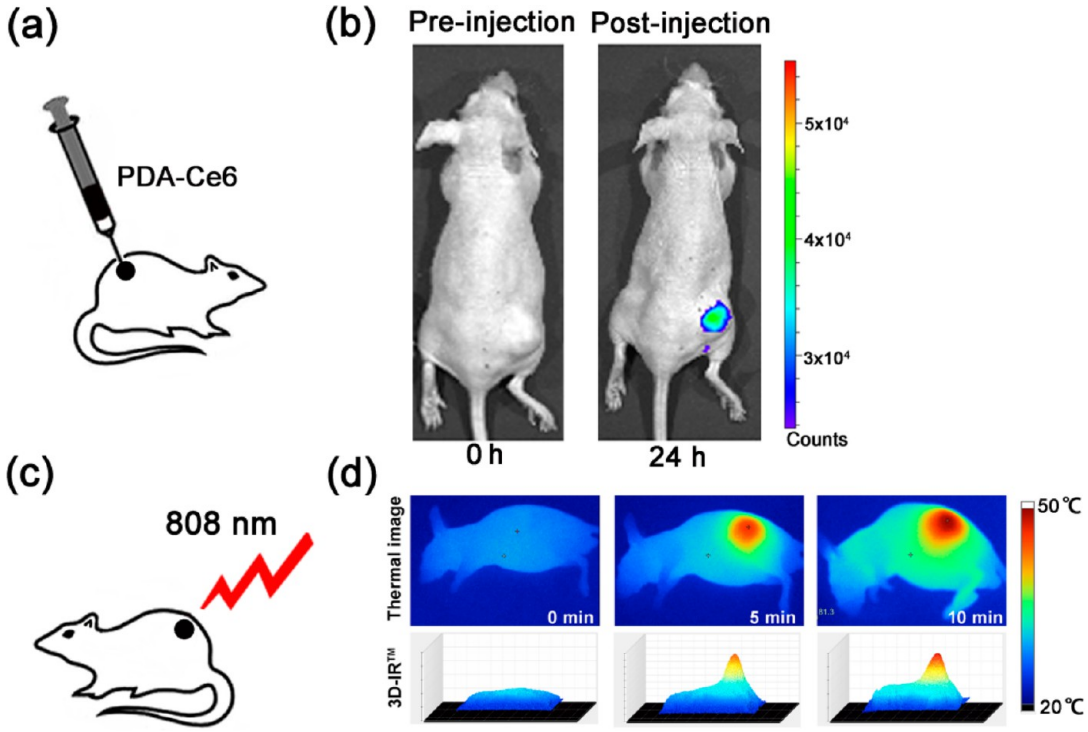

Figure 5. (a) Schematic view of HepG2 tumor-bearing nude mice with intratumoral injection of the PDA-Ce6 nanospheres. (b) *In vivo* NIR fluorescence image of HepG2 tumor-bearing nude mice after 24 h of injection. (c) Schematic view of HepG2 tumor-bearing nude mice which was receiving the 808 nm laser irradiation (2 W/cm^2) after 24 h of injection; (d) thermo-graphic images and the 3D temperature distribution of tumor-bearing nude mice that exposed to laser irradiation at 808 nm at different time points.

alone at 670 nm or the presence of PDA-Ce6 alone without laser irradiation could not induce any additional ROS production inside the tumor cells, which was indicated by almost the same fluorescence intensity in these groups, in comparison to the control group. Similarly, there was no more ROS generation in the cells treated with PDA-Ce6 nanospheres under the 808 nm laser irradiation, implying that the 808 nm laser used in PTT treatment could not be the appropriate wavelength for PDT. However, when the PDA-Ce6 treated cells irradiated by 670 nm laser, we could clearly see a very strong green fluorescence which is much higher than that of the free Ce6-treated cells, ascribing to the higher stability under physiological conditions and stronger cellular uptake of the PDA-Ce6 nanospheres (Figure 3d). These results proved that the ROS could be selectively generated in the PDA-Ce6 treated cells upon 670 nm NIR irradiation. Thus, the PDA-Ce6 nanospheres could be applied as a promising candidate for PDT treatment.

***In Vitro* Cytotoxicity Assay and Photodynamic/Photothermal-Induced Cell Death.** The photothermal conversion and the ROS generation ability of our PDA-Ce6 nanospheres prompt us to evaluate their feasibility as a PTT/PDT dual-modal agent for cancer phototherapy. Nontoxicity or low toxicity is a key criterion of any nanomaterials for biomedical applications. Here, the HepG2 liver cancer cells and Chang liver normal liver cells are taken as cell models to evaluate the cytotoxicity of the PDA-Ce6 nanospheres. As shown in Figure 4a and 4b, both of the PDA nanoparticles and PDA-Ce6 nanospheres showed a very low cytotoxic effect on these two types of cells in the absence of laser irradiation; even at a high dose of 8 μg/mL, the cells remained more than 90% viable after 24 h of incubation.

Afterward, the phototoxicity (PTT/PDT effects) of PDA-Ce6 nanospheres was analyzed by using Cell Counting Kit (CCK-8). As shown in Figure 4c, the PDA-Ce6 nanospheres showed a dose-dependent PDT effect under the 670 nm laser irradiation (50 mW/cm^2), and the cell viability decreased to 49.5% at the Ce6 concentration of 0.8 μg/mL, which was much lower than the cells treated with free Ce6 (71.6%) at the same concentration, because of the higher ROS generation in the PDA-Ce6 nanospheres incubated cells. In addition, the PDA-Ce6 nanospheres could also show a dose-dependent PTT effect under the 808 nm laser irradiation (2 W/cm^2) and the cell viability decreased to 41.6% at the Ce6 concentration of 0.8 μg/mL (equivalent PDA concentration, 3.2 μg/mL). More significantly, upon the combination of both NIR laser irradiation (670 nm, laser power intensity of 50 mW/cm^2 and 808 nm, laser power intensity of 2 W/cm^2), the cell viability of PDA-Ce6 treated cells was dramatically decreased. At a Ce6 concentration of 0.8 μg/mL in the PDA-Ce6 nanospheres, the cell viability was declined to 19%, which exhibited the excellent PDT/PTT combination effect of our nanospheres.

To further evaluate the localized photokilling effect of the combined NIR laser irradiation, HepG2 cells were incubated with PDA-Ce6 nanospheres (equivalent Ce6 concentration, 1 μg/mL) for 2 h and subsequently irradiated under the NIR laser. After treatment, the residual live cells were stained with Calcein AM, which could exhibit a green fluorescence. As shown in Figure 4d, the HepG2 cells showed entire vivid green fluorescence in the absence of laser irradiation, indicating low cytotoxicity of our PDA-Ce6 nanospheres. However, several cells could be killed within the laser spot via the ROS-induced apoptosis (PDT) upon the 670 nm laser irradiation. Besides the PDT effect, photothermal killing (PTT) could also be observed

DOI: 10.1021/acsami.5b01027
ACS Appl. Mater. Interfaces 2015, 7, 8176−8187

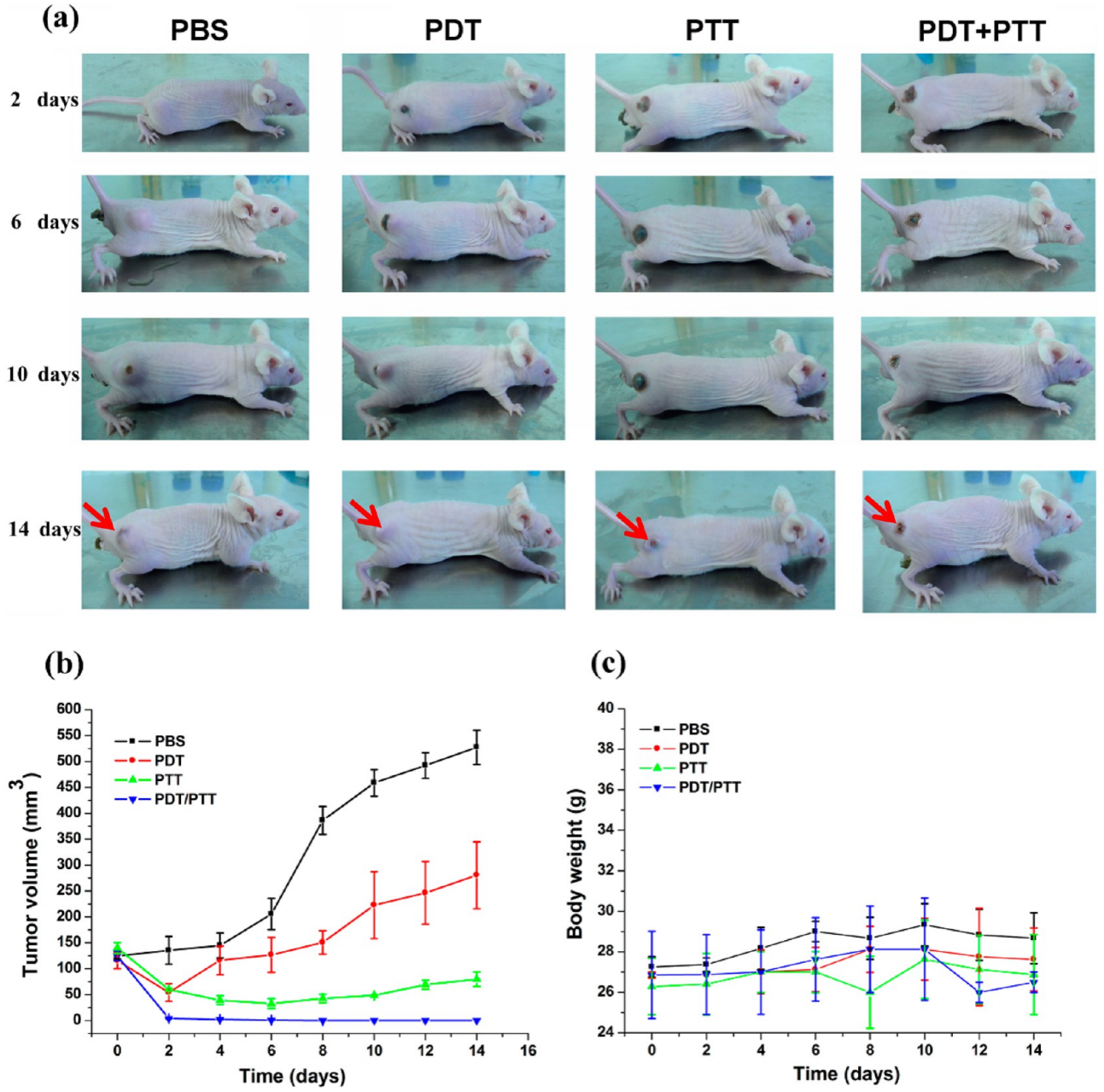

Figure 6. (a) *In vivo* therapeutic response to PDT (670 nm, 50 mW/cm^2), PTT (808 nm, 2 W/cm^2) treatment, and combined PDT/PTT treatment. (b) Tumor volumes of mice after different treatments as indicated. All data are presented as mean ± SD (n = 4). (c) Mean body weights of mice in different groups after treatment (n = 4).

and only a few treated cells remained alive within the laser spot upon the laser irradiation at 808 nm. In contrast, almost no surviving cells could be observed inside the laser spot with the combination irradiation by 670 and 808 nm lasers. These findings clearly demonstrated that our PDA-Ce6 nanospheres had excellent combined PDT/PTT effects against cancer cells.

The cell apoptosis induced by the photothermal/photodynamic treatment of PDA-Ce6 nanospheres was determined by flow cytometry using Annexin-V-FITC/PI staining. The stained cells were divided into four subgroups, and the viable group, the early apoptotic group, the late apoptotic/necrotic group and the dead cells/debris group, was localized in the lower left, lower right, upper right, and upper left quadrants, respectively. As shown in Figure 4e, the majority of cells were localized in the lower left quadrant with more than 94.15% of the viable cells in the control, which is indicating no apparent cell death. Compared with the control, most of the cells without PDA-Ce6 nanosphere treatment still remained alive (91.85% of the viable cells) under laser irradiation at both 670 and 808 nm. However, the percentage of viable cells was significantly decreased in the PDA-Ce6 nanosphere treated groups under either single laser irradiation or laser irradiation at both wavelengths (670 + 808 nm). As shown in Figure 4e, the percentage of viable cells was 65.21% or 72.07%, the percentages of apoptotic cells was 32.64% or 23.06%, and the percentage of dead cells was 2.15% and 4.88% under laser irradiation at 670 or 808 nm, respectively. Although the percentage of apoptotic cells was not significantly changed (32.93%) under laser irradiation using both wavelengths (670 nm + 808 nm), compared to single laser irradiation, the

DOI: 10.1021/acsami.5b01027
ACS Appl. Mater. Interfaces 2015, 7, 8176−8187

percentage of viable cells under laser irradiation at both wavelengths (670 nm + 808 nm) was significantly decreased to 55.61%, and the percentage of dead cells was significantly increased to 11.46%. These results clearly demonstrated the combined cell killing efficiency or the combined PDT and PTT effects of our PDA-Ce6 nanospheres.

***In Vivo* Photodynamic/Photothermal Therapy.** The PDT/PTT combination therapeutic efficacy of the PDA-Ce6 nanospheres was further examined in tumor-bearing nude mice. To monitor the stable distribution of the PDA-Ce6 nanospheres in the tumor site, the entire body fluorescence images collected by the IVIS Series Preclinical In Vivo Imaging Systems (Perkin−Elmer) were obtained after 24 h of intratumoral injection. As shown in Figure 5b, comparing to the preinjected images, the mice only showed strong fluorescence signals corresponding to the fluorescence of Ce6 conjugated at the surface of PDA at the tumor site but not in the entire body, which implied that most of the nanospheres were still localized inside the tumor even after 24 h of injection. Meanwhile, the fluorescence images of the tumors and major organs that were harvested from the sacrificed mice after intratumoral injection are shown in Figure S8 in the Supporting Information, and the results also clearly demonstrated that the PDA-Ce6 nanospheres were still retained inside the tumor site after 24 h of injection. Moreover, the NIR laser-induced whole body temperature distribution images were investigated by an infrared (IR) thermal camera. As shown in Figure 5d, upon the 808 nm NIR laser irradiation, the local temperature of the PDA-Ce6 injected tumor rapidly increased above 50 °C, which is high enough to ablate the malignant cells, while no significant temperature changes were observed in other parts of the mice.

Next, we further investigated the PDT/PTT combination therapeutic efficacy *in vivo*; changes in the tumor volumes of the four group mice that received various treatments (as mentioned in the Experimental Section) were monitored for 14 days. As shown in Figures 6a and 7a, mice experienced a rapid growth of tumor volume in group 1, indicating that only the use of laser irradiation without PDA-Ce6 has no influence on the tumor growth. In contrast, PDA-Ce6 administration/irradiation groups (groups 2, 3, and 4) showed remarkable delays in tumor growth or even tumor regression after 14 days, indicating the photoinduced therapeutic effects or our nanospheres. However, it is noteworthy that group 4 exhibited much higher therapeutic efficiency, compared with group 2 and group 3 on day 14, and the tumors in group 4 were almost completely destroyed with only scar tissue remaining after 2 weeks of treatment (see Figures 6a and 6b). These results clearly demonstrated the combined effects of PDT/PTT over any single modality treatment. Since high toxicity usually leads to weight loss, we also measured the body weight of the mice for all groups during the treatments, and no obvious weight loss was observed (Figure 6c), implying that the toxicity or side effects of our nanospheres were not serious.

Furthermore, the antitumor efficacy was also evaluated by H&E staining of tumor tissues after 24 h of treatment. Tumor tissues from mice in group 1, as mentioned above, were used as control. As shown in Figure 7b, no necrosis or obvious apoptosis was observed in the tumor tissue slices, and the tumor cells retained their normal morphology with distinguishable membrane and nuclear structure (Figure 7b). The tumors that received PDT (group 2) or PTT (group 3) treatment alone showed a certain degree of tissue and cellular damage, due to the apoptosis of cancer cells induced by the PDT or PTT effect alone. However, the combined PDT/PTT treatment mice in group 4 showed significant cell destruction and extensive damaged areas, as indicated by the loss of tissue architectures and decreased general intensity of tissues. Meanwhile, the immunohistochemical (IHC) staining of tumor sections for antigen Ki67 was used to evaluate cell proliferation. The Ki67 was significantly positive expressed in the control mice, as indicated by the brown granules in the cell nucleus. As expected, the Ki67 signal from the tumor cells that received the combined treatment of PDT and PTT (group 4) was much weaker than other groups (Figure 7c). These data clearly demonstrated that our PDA-Ce6 nanospheres could serve as a highly effective PDT/PTT dual-modal therapeutic agent.

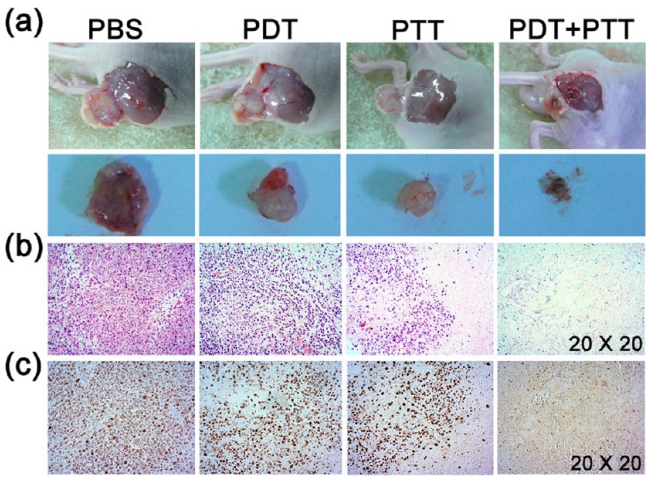

Figure 7. (a) Anatomical structure of HepG2 tumors in the subcutaneous space at day 14 after different treatments (as indicated). (b) Corresponding H&E staining of the tumor tissues after 24 h treatment as indicated. (c) Immunohistochemical staining of the tumor tissues after treatment for 24 h (as indicated).

CONCLUSION

In conclusion, a PDT/PTT dual-modal therapeutic agent based on Ce6 modified poly(dopamine) nanospheres was successfully synthesized. The PDA-Ce6 nanospheres exhibited excellent biocompatibility and little toxicity, as well as high ROS generation and high photothermal conversion efficiencies. The antitumor efficiency of the PDA-Ce6 nanospheres upon the NIR laser irradiation was also carefully evaluated both *in vitro* and *in vivo*, and the results showed that antitumor efficiency could be significantly enhanced by the combination of PTT/PDT treatment by using dual-wavelength (670 nm, 808 nm) laser irradiation. Therefore, our prepared PDA-Ce6 nanospheres might be a very promising dual-mode PDT/PTT therapeutic agent for future cancer therapy.

ASSOCIATED CONTENT

Supporting Information

Supporting Information available: additional ^{13}C solid-state NMR spectra of PDA nanoparticles, FT-IR spectra of PDA nanoparticles, DLS profiles and zeta potentials of PDA nanoparticles and PDA-Ce6 nanospheres, chromatograms of the standard Ce6, the peak area of various concentration of Ce6 at the retention time of 11.66 min; the absorbance of 9,10-dimethylanthracene (ABDA, 20 mM) after photodecomposition by ROS generation upon NIR laser irradiation, photograph

DOI: 10.1021/acsami.5b01027
ACS Appl. Mater. Interfaces 2015, 7, 8176−8187

and fluorescence images of tumors and main organs harvested from tumor-bearing mice after 24 h of intratumoral injection. This material is available free of charge via the Internet at http://pubs.acs.org.

AUTHOR INFORMATION

Corresponding Authors

*E-mail: xiaoloong.liu@gmail.com (X. Liu).
*E-mail: drjingfeng@126.com (J. Liu).

Notes

The authors declare no competing financial interest.

ACKNOWLEDGMENTS

This work is supported by the key clinical specialty discipline construction program of Fujian, PRC; the National Natural Science Foundation of China (Grant No. 31201008); the specialized Science and Technology Key Project of Fujian Province (Grant No. 2013YZ0002-3); the Scientific Foundation of Fuzhou Health Department (Grant Nos. 2014-S-w18 and 2014-S-w25); and the Backbone Talents Training Project of Fujian Health Department (Grant No. 2013-ZQN-ZD-29).

REFERENCES

(1) Pegaz, B.; Debefve, E.; Borle, F.; Ballini, J. P.; van den Bergh, H.; Kouakou-Konan, Y. N. Encapsulation of Porphyrins and Chlorins in Biodegradable Nanoparticles: The Effect of Dye Lipophilicity on the Extravasation and the Photothrombic Activity. A Comparative Study. *J. Photochem. Photobiol., B* **2005**, *80*, 19−27.

(2) Bonnett, R.; Martinez, G. Photobleaching of Sensitisers Used in Photodynamic Therapy. *Tetrahedron* **2001**, *57*, 9513−9547.

(3) Talreja, J. P.; DeGaetani, M.; Sauer, B. G.; Kahaleh, M. Photodynamic Therapy for Unresectable Cholangiocarcinoma: Contribution of Single Operator Cholangioscopy for Targeted Treatment. *Photochem. Photobiol. Sci.* **2011**, *10*, 1233−1238.

(4) Bugaj, A. M. Targeted Photodynamic Therapy—A Promising Strategy of Tumor Treatment. *Photochem. Photobiol. Sci.* **2011**, *10*, 1097−1109.

(5) Kim, J.-Y.; Choi, W. I.; Kim, M.; Tae, G. Tumor-Targeting Nanogel That Can Function Independently for Both Photodynamic and Photothermal Therapy and Its Synergy from the Procedure of PDT Followed by PTT. *J. Controlled Release* **2013**, *171*, 113−121.

(6) Paszko, E.; Ehrhardt, C.; Senge, M. O.; Kelleher, D. P.; Reynolds, J. V. Nanodrug Applications in Photodynamic Therapy. *Photodiagn. Photodyn. Ther.* **2011**, *8*, 14−29.

(7) Gandjbakhche, A. H.; Chernomordik, V.; Hattery, D.; Hassan, M.; Gannot, I. Tissue Characterization by Quantitative Optical Imaging Methods. *Technol. Cancer Res. Treat.* **2003**, *2*, 537−551.

(8) Celli, J. P.; Spring, B. Q.; Rizvi, I.; Evans, C. L.; Samkoe, K. S.; Verma, S.; Pogue, B. W.; Hasan, T. Imaging and Photodynamic Therapy: Mechanisms, Monitoring, and Optimization. *Chem. Rev.* **2010**, *110*, 2795−2838.

(9) Richter, A. M.; Waterfield, E.; Jain, A. K.; Canaan, A. J.; Allison, B. A.; Levy, J. G. Liposomal Delivery of a Photosensitizer, Benzoporphyrin Derivative Monoacid Ring A (BPD), to Tumor Tissue in a Mouse Tumor Model. *Photochem. Photobiol.* **1993**, *57*, 1000−1006.

(10) Miao, W.; Shim, G.; Lee, S.; Lee, S.; Choe, Y. S.; Oh, Y.-K. Safety and Tumor Tissue Accumulation of Pegylated Graphene Oxide Nanosheets for Co-Delivery of Anticancer Drug and Photosensitizer. *Biomaterials* **2013**, *34*, 3402−3410.

(11) Lee, S. J.; Koo, H.; Jeong, H.; Huh, M. S.; Choi, Y.; Jeong, S. Y.; Byun, Y.; Choi, K.; Kim, K.; Kwon, I. C. Comparative Study of Photosensitizer Loaded and Conjugated Glycol Chitosan Nanoparticles for Cancer Therapy. *J. Controlled Release* **2011**, *152*, 21−29.

(12) Moret, F.; Scheglmann, D.; Reddi, E. Folate-targeted PEGylated Liposomes Improve the Selectivity of PDT with Meta-Tetra (hydroxyphenyl) Chlorin (*m*-THPC). *Photochem. Photobiol. Sci.* **2013**, *12*, 823−834.

(13) Ling, D.; Bae, B. C.; Park, W.; Na, K. Photodynamic Efficacy of Photosensitizers Under an Attenuated Light Dose via Lipid Nano-Carrier-Mediated Nuclear Targeting. *Biomaterials* **2012**, *33*, 5478−5486.

(14) Wang, D.; Qian, J.; He, S.; Park, J. S.; Lee, K. S.; Han, S.; Mu, Y. Aggregation-enhanced Fluorescence in PEGylated Phospholipid Nanomicelles for *In Vivo* Imaging. *Biomaterials* **2011**, *32*, 5880−5888.

(15) Zeng, Y.; Zhang, D.; Wu, M.; Liu, Y.; Zhang, X.; Li, L.; Li, Z.; Han, X.; Wei, X.; Liu, X. Lipid-AuNPs@ PDA Nanohybrid for MRI/CT Imaging and Photothermal Therapy of Hepatocellular Carcinoma. *ACS Appl. Mater. Interfaces* **2014**, *6*, 14266−14277.

(16) Robinson, J. T.; Tabakman, S. M.; Liang, Y.; Wang, H.; Sanchez Casalongue, H.; Vinh, D.; Dai, H. Ultrasmall Reduced Graphene Oxide with High Near-Infrared Absorbance for Photothermal Therapy. *J. Am. Chem. Soc.* **2011**, *133*, 6825−6831.

(17) Antaris, A. L.; Robinson, J. T.; Yaghi, O. K.; Hong, G.; Diao, S.; Luong, R.; Dai, H. Ultra-low Doses of Chirality Sorted Carbon Nanotubes for Simultaneous Tumor Imaging and Photothermal Therapy. *ACS Nano* **2013**, *7*, 3644−3652.

(18) Choi, W. I.; Kim, J.-Y.; Kang, C.; Byeon, C. C.; Kim, Y. H.; Tae, G. Tumor Regression *In Vivo* by Photothermal Therapy Based on Gold-Nanorod-Loaded, Functional Nanocarriers. *ACS Nano* **2011**, *5*, 1995−2003.

(19) Jang, B.; Park, J. Y.; Tung, C. H.; Kim, I. H.; Choi, Y. Gold Nanorod− Photosensitizer Complex for Near-Infrared Fluorescence Imaging and Photodynamic/Photothermal Therapy *In Vivo*. *ACS Nano* **2011**, *5*, 1086−1094.

(20) Li, K.; Yamamoto, M.; Chan, S. J.; Chiam, M. Y.; Qin, W.; Wong, P. T.; Yim, E. K.; Tang, B. Z.; Liu, B. Organic Nanoparticles with Aggregation-Induced Emission for Tracking Bone Marrow Stromal Cells in the Rat Ischemic Stroke Model. *Chem. Commun.* **2014**, *50*, 15136−9.

(21) Tang, S.; Huang, X.; Zheng, N. Silica Coating Improves the Efficacy of Pd Nanosheets for Photothermal Therapy of Cancer Cells Using Near Infrared Laser. *Chem. Commun.* **2011**, *47*, 3948−3950.

(22) Terentyuk, G.; Panfilova, E.; Khanadeev, V.; Chumakov, D.; Genina, E.; Bashkatov, A.; Tuchin, V.; Bucharskaya, A.; Maslyakova, G.; Khlebtsov, N. Gold Nanorods with a Hematoporphyrin-Loaded Silica Shell for Dual-Modality Photodynamic and Photothermal Treatment of Tumors *In Vivo*. *Nano Res.* **2014**, *7*, 325−337.

(23) Lin, J.; Wang, S.; Huang, P.; Wang, Z.; Chen, S.; Niu, G.; Li, W.; He, J.; Cui, D.; Lu, G. Photosensitizer-loaded Gold Vesicles with Strong Plasmonic Coupling Effect for Imaging-Guided Photothermal/Photodynamic Therapy. *ACS Nano* **2013**, *7*, 5320−5329.

(24) Black, K. C.; Yi, J.; Rivera, J. G.; Zelasko-Leon, D. C.; Messersmith, P. B. Polydopamine-Enabled Surface Functionalization of Gold Nanorods for Cancer Cell-Targeted Imaging and Photothermal Therapy. *Nanomedicine* **2013**, *8*, 17−28.

(25) Lin, L.-S.; Cong, Z.-X.; Cao, J.-B.; Ke, K.-M.; Peng, Q.-L.; Gao, J.; Yang, H.-H.; Liu, G.; Chen, X. Multifunctional Fe_3O_4@ Polydopamine Core−Shell Nanocomposites for Intracellular mRNA Detection and Imaging-Guided Photothermal Therapy. *ACS Nano* **2014**, *8*, 3876−3883.

(26) Liu, Y.; Ai, K.; Liu, J.; Deng, M.; He, Y.; Lu, L. Dopamine-Melanin Colloidal Nanospheres: An Efficient Near-Infrared Photothermal Therapeutic Agent for *In Vivo* Cancer Therapy. *Adv. Mater.* **2013**, *25*, 1353−1359.

(27) Wu, M.; Zhang, D.; Zeng, Y.; Wu, L.; Liu, X.; Liu, J. Nanocluster of Superparamagnetic Iron Oxide Nanoparticles Coated with Poly(dopamine) for Magnetic Field-Targeting, Highly Sensitive MRI and Photothermal Cancer Therapy. *Nanotechnology* **2015**, *26*, 115102.

(28) Yan, J.; Yang, L.; Lin, M. F.; Ma, J.; Lu, X.; Lee, P. S. Polydopamine Spheres as Active Templates for Convenient Synthesis of Various Nanostructures. *Small* **2013**, *9*, 596−603.

(29) Isakau, H.; Trukhacheva, T.; Zhebentyaev, A.; Petrov, P. HPLC Study of Chlorin e_6 and Its Molecular Complex with Polyvinylpyrrolidone. *Biomed. Chromatogr.* **2007**, *21*, 318−325.

DOI: 10.1021/acsami.5b01027
ACS Appl. Mater. Interfaces 2015, 7, 8176−8187

(30) Della Vecchia, N. F.; Avolio, R.; Alfè, M.; Errico, M. E.; Napolitano, A.; d'Ischia, M. Building-Block Diversity in Polydopamine Underpins a Multifunctional Eumelanin-Type Platform Tunable through a Quinone Control Point. *Adv. Funct. Mater.* **2013**, *23*, 1331−1340.
(31) Liu, X.; Cao, J.; Li, H.; Li, J.; Jin, Q.; Ren, K.; Ji, J. Mussel-Inspired Polydopamine: A Biocompatible and Ultrastable Coating for Nanoparticles *In Vivo*. *ACS Nano* **2013**, *7*, 9384−9395.
(32) Idris, N. M.; Gnanasammandhan, M. K.; Zhang, J.; Ho, P. C.; Mahendran, R.; Zhang, Y. *In Vivo* Photodynamic Therapy Using Upconversion Nanoparticles as Remote-Controlled Nanotransducers. *Nat. Med.* **2012**, *18*, 1580−1585.
(33) Pass, H. I. Photodynamic Therapy in Oncology: Mechanisms and Clinical Use. *J. Natl. Cancer Inst.* **1993**, *85*, 443−456.

DOI: 10.1021/acsami.5b01027
ACS Appl. Mater. Interfaces 2015, 7, 8176−8187